Control of Tetrahedral Coordination and Superconductivity in $FeSe_{0.5}Te_{0.5}$ Thin Films

S. X. Huang,[1] C. L. Chien,[1] V. Thampy,[1,2] and C. Broholm[1,2,3]

[1]*Department of Physics and Astronomy, The Johns Hopkins University, Baltimore, Maryland 21218, USA*
[2]*Institute for Quantum Matter, The Johns Hopkins University, Baltimore, Maryland 21218, USA*
[3]*NIST Center for Neutron Research, National Institute of Standards and Technology, Gaithersburg, Maryland 20899, USA*

(Received 18 January 2010; published 25 May 2010)

We demonstrate a close relationship between superconductivity and the dimensions of the Fe-Se(Te) tetrahedron in $FeSe_{0.5}Te_{0.5}$. This is done by exploiting thin film epitaxy, which provides controlled biaxial stress, both compressive and tensile, to distort the tetrahedron. The Se/Te height within the tetrahedron is found to be of crucial importance to superconductivity, in agreement with the scenario that (π, π) spin fluctuations promote superconductivity in Fe superconductors.

DOI: 10.1103/PhysRevLett.104.217002 PACS numbers: 74.70.Xa, 74.25.F−, 74.78.−w

The discovery of Fe based superconductors (Fe-SC) in 2008 [1–3] has captured intense attention. To the surprise of many, the pairing symmetry of the Fe-SC appears to be not d wave as in high T_C cuprates, but s wave [4]. One leading theoretical proposal for Fe-SCs has $s_{\pm}$ pairing symmetry [5–8]. The mechanism for Fe based superconductivity appears to be different from previously known superconductors and rooted in their crystal structures [6,9–11]. Fe-SCs contain a puckered FeAs(Se) sheet consisting of a two-dimensional Fe square lattice with the As (or Se) atoms located at the square centers protruding alternatively above and below the Fe plane. Unique among the Fe-SCs is the FeSe (“11”) superconductor which contains only the essential FeSe sheet.

The puckered FeAs(Se) sheets in all Fe-SCs consist of Fe-As(Se) tetrahedrons. The tetrahedral configuration is of crucial importance to Fe-SCs and can be advantageously investigated in FeSe. FeSe has a tetragonal crystal structure with lattice parameters a and c as shown in the Fig. 1(b). The four Se atoms located above and below the Fe plane at a height of $h = zc$ form a tetrahedron characterized by the Fe-Se bond length of $(a^2/4 + z^2c^2)^{1/2}$, the Se-Fe-Se bond angle of $\alpha = 2\tan^{-1}(a/2zc)$, the Se-Se interlayer separation in the c direction of $c_{\text{Se-Se}} = c(1 - 2z)$, and the Se-Se distance of $d_{\text{Se-Se}} = [a^2/2 + c^2_{\text{Se-Se}}]^{1/2}$.

Our goal is to examine the relationship between these tetrahedral dimensions and superconductivity for a single composition. High-pressure measurements and strained epitaxial thin films are possible methods but not chemical substitution, which alters the electronic properties in addition to structure. In this work, we have exploited epitaxial $FeSe_{0.5}Te_{0.5}$ thin films to address the crucial roles of the tetrahedral coordination. We find that the superconducting transition temperature in $FeSe_{0.5}Te_{0.5}$ thin films is directly linked to the height zc, as predicted [9] if (π, π) spin fluctuations promote superconductivity.

Superconducting $FeSe_{1-x}Te_x$ thin films were recently reported [12–16]. In our case, 400(±50) nm thin films were grown on (100)MgO with a range of substrate temperatures (T_S) by pulsed laser (248 nm KrF excimer) ablation of $FeSe_{0.5}Te_{0.5}$ targets which were fabricated by a two-step process [17]. The $\theta/2\theta$ x-ray diffraction pattern [Fig. 1(a)] shows only the (00l) peaks illustrating that all the $FeSe_{0.5}Te_{0.5}$ films have exclusively c-axis orientation. As shown in Fig. 1(c), with increasing T_S, the lattice parameter c decreases monotonically. Remarkably, c is

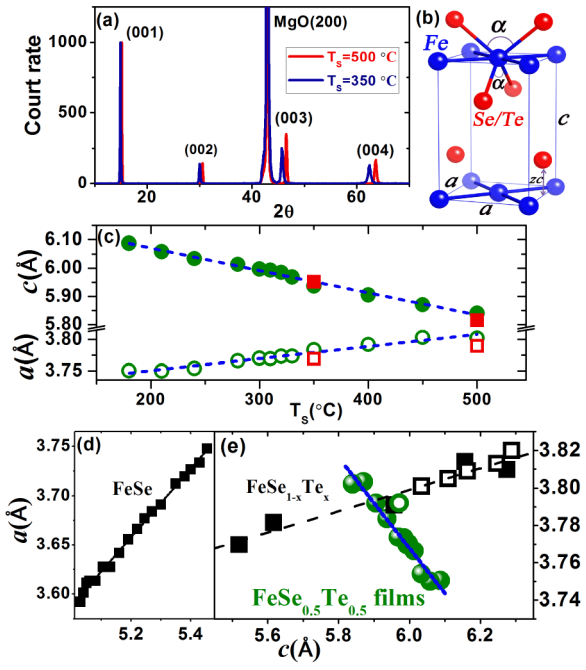

FIG. 1 (color online). (a) XRD patterns [normalized to (001) peak] of $FeSe_{0.5}Te_{0.5}$ films deposited at 350 °C and 500 °C on (100)MgO. (b) Structure of $FeSe_{1-x}Te_x$ with lattice constants a and c, Se/Te position cz and bond angle α. (c) c and a of $FeSe_{0.5}Te_{0.5}$ films as a function of T_S. Square symbols are from neutron diffraction. (d) Variation of a and c of FeSe under high pressure (Ref. [20]) (e) Variation of lattice constant a and c of $FeSe_{0.5}Te_{0.5}$ thin films (solid circles), target (open circles) and bulk $FeSe_{1-x}Te_x$ (solid squares, Ref. [23], open squares, Ref. [24]).

linearly dependent on T_S. The lattice parameter a can be deduced from the d spacing of the (101) peak at tilted geometry via the relation of $1/d_{101}{}^2 = 1/a^2 + 1/c^2$. Measurements of the (200) peak and the (00l) peaks for two of the samples by neutron diffraction gave consistent values for a and c as shown in Fig. 1(c). The lattice parameter a increases quasi linearly with T_S while maintaining the unit cell volume unchanged to within 1%. The evolution of stress with substrate temperature can be understood as follows. At low T_S, the compressive stress is built in during polycrystalline film thickening [18]. Increased diffusion as higher T_S relieves the compressive stress [19]. At high T_S, thermal stress takes over, and it is tensile due to the higher thermal expansion coefficient of $FeSe_{1-x}Te_x$ than that of the MgO substrate. T_S thus avails itself as a unique tool to apply biaxial stress resulting in a linear strain of the films. This is distinct from high-pressure experiments [20,21], where both a, c, and the volume are reduced from ambient values, and from substitution experiments [10,22–24], where c generally scales with a. Indeed, as shown in Fig. 1(e) (solid circles), epitaxial $FeSe_{0.5}Te_{0.5}$ films allow exploration of regions of lattice constants for a single composition, which cannot be accessed by other means.

The substrate temperature T_S plays a key role in epitaxy, which we determined using pole-figures and in-plane ϕ scan about the (101) peak. For $T_S \approx 500\,^\circ$C, the thin films are exclusively $\langle 100\rangle FeSe_{0.5}Te_{0.5}||\langle 100\rangle MgO$ with excellent epitaxy (FWHM of $\Delta\phi \sim 2^\circ$) [Fig. 2(a)]. This epitaxy evolves into a mixture of an increasing amount of $\langle 100\rangle FeSe_{0.5}Te_{0.5}||\langle 110\rangle MgO$ at $T_S \approx 400\,^\circ$C [Fig. 2(b)]. At $T_S = 280\,^\circ$C, the basal plane of $FeSe_{0.5}Te_{0.5}$ is rotated by 45° around c with respect to that of MgO ($\langle 100\rangle FeSe_{0.5}Te_{0.5}||\langle 110\rangle MgO$) as indicated by Fig. 2(c). For $T_S \leq 180\,^\circ$C [Fig. 2(d)] only nonepitaxial growth is observed.

The conducting and superconducting properties of the $FeSe_{0.5}Te_{0.5}$ films also depend sensitively on T_S as shown in Fig. 3. Samples deposited at high T_S (>400 °C) show semiconducting behavior, while those deposited at lower T_S (< 400 °C) are metallic. More importantly, the resistivity ratio and T_C vary systematically but *not* monotonically with T_S. Starting with $T_S \approx 180\,^\circ$C, T_C gradually shifts to higher temperature with increasing T_S. The maximum values of $T_C = 10.75$ K is reached at $T_S \approx 310\,^\circ$C. While improving epitaxy, increasing T_S however degrades superconductivity and eventually produces semiconducting films. Recent c-axis oriented polycrystalline $FeSe_{0.5}Te_{0.5}$ films [25] show similar dependence of lattice parameters and superconducting properties on T_S, suggesting that in-plane epitaxy may not be of overriding importance.

We shall now show that the dramatic changes in the conducting properties of the $FeSe_{0.5}Te_{0.5}$ thin films deposited at different T_S originate from the variation in the crystal structure and especially the tetrahedral coordination. In addition to a and c, the determination of the all-important Fe-Se tetrahedrons requires determination of z, which can be obtained from the integrated intensities I_{00l} of the (00l) peaks, especially that of the (003) peak. For constant sample illumination area, the x-ray $\theta - 2\theta$ integrated intensity I_{00l} for a thin film can be expressed as follows [26]:

$$I_{00l} = A \cdot f(p) R_{||}(\theta)(1 + \cos^2 2\theta)|F(z)_{00l}|^2 \times \left(1 - \exp\left(-\frac{2\mu t}{\sin\theta}\right)\right) \quad (1)$$

where A is a prefactor, $f(p)$ is the dynamic correction factor [26], $R_{||}(\theta)$ is a sensitivity factor for $\theta - 2\theta$ scans [27], $F(z)_{00l}$ is the structure factor, μ is the linear attenuation coefficient, and t is the thickness of the thin films. We also carried out $E_i = 30.5$ meV neutron diffraction on two of the samples. The corresponding expression for rocking scan integrated intensity reads $I_{00l} = A \cdot R_\perp(\theta)|F(z)_{00l}|^2$.

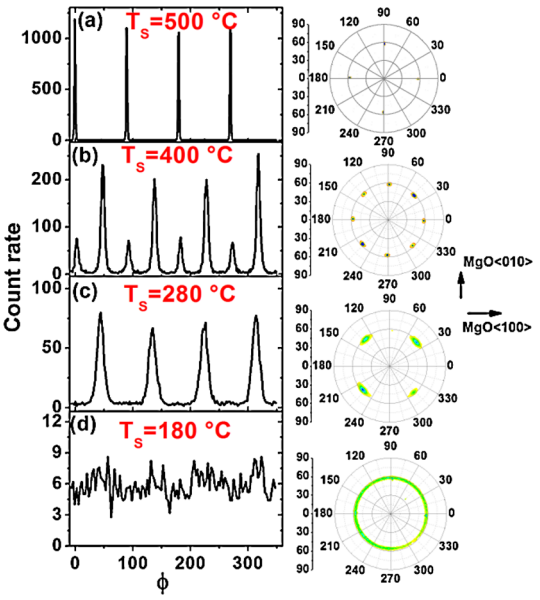

FIG. 2 (color online). In-plane ϕ scan (left) and corresponding pole figures (right) about the (101) peak of $FeSe_{0.5}Te_{0.5}$ thin films deposited at various substrate temperatures.

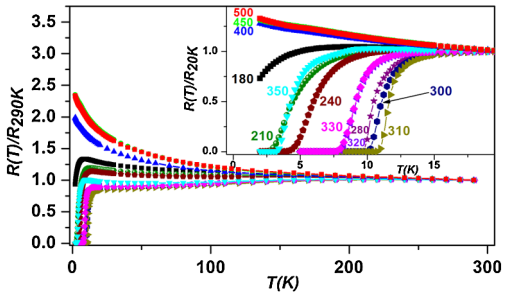

FIG. 3 (color online). Normalized resistance as a function of temperature for $FeSe_{0.5}Te_{0.5}$ films. Inset: Resistance (normalized to that at $T = 20$ K) at various T_S as indicated.

To extract z from the neutron and x-ray diffraction data we minimized the profile parameter R_{wp} by varying A and z:

$$R_{wp} = \left[\frac{\sum_{l=1}^{4}(I_{00l}^{obs.} - I_{00l}^{cal.}(z))^2}{\sum_{l=1}^{4}(I_{00l}^{obs.})^2}\right]^{1/2} \quad (2)$$

The top right inset to Fig. 4(a) shows observed versus fitted integrated intensities for neutron and x-ray diffraction from the $T_s = 350\,^{\circ}\mathrm{C}$ sample. Clustered around the diagonal and with R_{wp} values of 6% and 17%, respectively. The values of z, however, are not consistent to within error bars: $z(350\,^{\circ}\mathrm{C}$, neutron$) = 0.263(2)$, whereas $z(350\,^{\circ}\mathrm{C}$, x-ray$) = 0.283(3)$. This indicates that the relatively small number of peaks that could be detected from the thin film samples is insufficient to obtain reliable absolute z values. However, the bottom left inset to Fig. 4(a) shows that the relative integrated x-ray intensity I_{003}/I_{001} depends sensitively on Δz, the change in z with respect to a chosen reference sample. Assuming that all relevant sample dependence of the integrated intensity is associated with Δz, we extracted this quantity by fitting such data in an analysis that now is completely independent of the prefactors in Eq. (1). The consistency of neutron and x-ray data in this analysis provides confidence that the values extracted for Δz are reliable.

We now discuss c, a, and Δz which characterize strain induced changes at the atomic scale. While c increases with decreasing substrate temperature [Fig. 1(c)] $\Delta h_{Se/Te} = c\Delta z + z\Delta c$ decreases monotonically [Fig. 4(b)] by a total of 0.08(2) Å. For $c > 6.02$ Å (with $T_S < 280\,^{\circ}\mathrm{C}$), the z value continues to decrease though overlap of the (003) peak with the much more intense MgO(200) peak [Fig. 1(a)] eventually reduces the experimental accuracy. Thus, in response to a compressive biaxial stress, while the lattice constant c expands, the height $2zc$ of the tetrahedron in the c direction actually *contracts*. This is *opposite* to the behavior under hydrostatic pressure [20]. As a consequence, the interlayer distance $d_{Se\text{-}Se}$ increases with c as shown in Fig. 4(b). The overall transport properties of the $FeSe_{0.5}Te_{0.5}$ films vary systematically with c and the corresponding changes in tetrahedral Fe-Se/Te coordination. This is quantitatively displayed in Fig. 4(c) by plotting $RR = R^{onset}/R(T = 290\ \mathrm{K})$ (where R^{onset} is defined as the value of onset of superconductivity, or $T = 2$ K) as the open circles, which vary systematically with c. For samples with $c < 5.92$ Å (at high T_S) and $c > 6.02$ Å (at low T_S) the samples show semiconducting behavior at low temperature with $RR > 1$. In between lie the superconducting samples for which the value of T_C distinctively anticorrelates with RR showing a maximum at $c \approx 6$ Å. Rather than directly associated with the changes in c, this variation of superconductivity may be linked to changes in the iron coordinating Se/Te tetrahedron.

One characteristic of possible importance is the Fe-As (Se)-Fe bond angle α, which for an ideal and undistorted tetrahedron is 109.5°. This angle is indeed realized in the optimally doped and highest T_c "1111" and "122" Fe-SCs

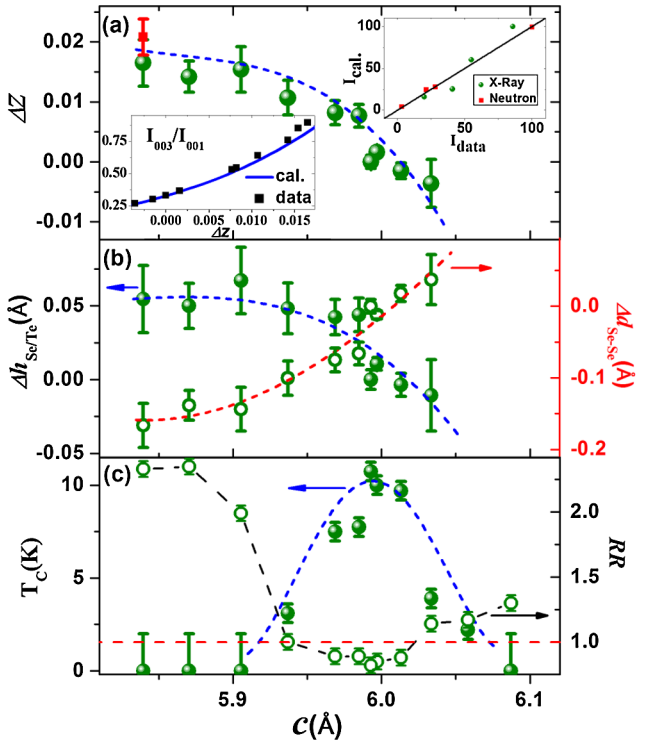

FIG. 4 (color online). Variation of structural parameters (a) Δz, (b) $\Delta h_{Se/Te}$ (Solid circles) and $\Delta d_{Se\text{-}Se}$ (Open circles) for samples synthesized with different T_s relative to the reference sample $T_r = 310\,^{\circ}\mathrm{C}$: $\Delta z(T_S) = z(T_S) - z(T_r)$ etc. Square symbol is from neutron diffraction ($z(500\,^{\circ}\mathrm{C}$, neutron$) - z(350\,^{\circ}\mathrm{C}$, neutron$) + \Delta z(350\,^{\circ}\mathrm{C}$, x-ray$)$). (c) T_C (solid circles) and resistance ratio RR (open circles, see text for definition) of $FeSe_{0.5}Te_{0.5}$ films as a function of c. Top right inset in (a) shows the measured versus modeled neutron and x-ray integrated intensity for the $T_s = 350\,^{\circ}\mathrm{C}$ sample. Bottom left inset shows the measured (square) and modeled (line) I_{003}/I_{001} as a function of Δz. All dashed lines are guides to eyes.

[10]. However, in bulk FeSe with $T_C \approx 8$ K, α is less at 104°, and in bulk $FeSe_{0.5}Te_{0.5}$ with $T_C \approx 12$ K α is even smaller at about 99° [10]. In the high-pressure measurements of bulk FeSe [20], α is only slightly reduced, yet T_C is greatly enhanced to 37 K. In the present case of thin films of a single composition $FeSe_{0.5}Te_{0.5}$, because both a and zc decrease with increasing c, the bond angle α remains roughly unchanged at about 98°, while the superconductivity varies greatly. These results suggest that the bond angle α does not significantly influence T_C.

The other two structural characteristics of importance are the chalcogen height $h_{Se/Te} = zc$and Se-Se separation $d_{Se\text{-}Se}$. For increasing c, z and $h_{Se\text{-}Te}$ decrease monotonically. As a result, both $d_{Se\text{-}Se}$ [Fig. 4(b), open circles] and $c_{Se\text{-}Se}$ (not shown) increase monotonically. Hence, while the c axis expands, the tetrahedron undergoes compressive distortion such that the essential FeSe(Te) plane becomes "thinner" and further separated from its neighboring planes. Concomitant to the structural variations is the evolution of superconductivity. As shown in Fig. 5, with

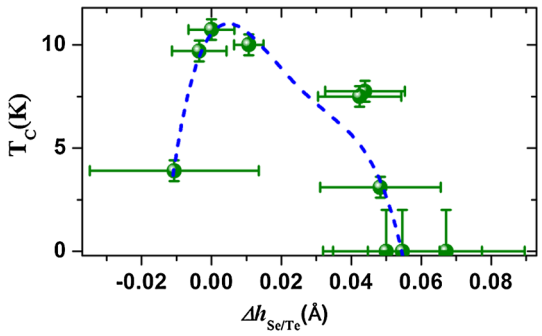

FIG. 5 (color online). T_C as a function of height $\Delta h_{Se/Te}$ relative to the reference sample. Dashed line is guide to eyes.

decreasing $\Delta h_{Se/Te}$, T_C first appears at $\Delta h_{Se/Te} \approx 0.05$ Å. As $\Delta h_{Se/Te}$ further decreases, the value of T_C increases and reaches a maximum at $\Delta h_{Se/Te} \sim 0$ Å—the reference sample ($h = 1.631(7)$ Å, x-ray) which we expect to be similar to bulk $FeSe_{0.493}Te_{0.507}$ where $h = 1.619(3)$ Å [28]. Superconductivity in Fe-SC is generally believed to be magnetic in origin. In particular, the so-called (π, π) spin fluctuation, promoting interband scattering between the hole and the electron pockets [29], gives rise to superconducting pairing [29,30]. It has recently been shown theoretically [9] that the chalcogen height has a strong influence on the stability of magnetic ground state; as Te(Se) height is lowered, superexchange interaction between Fe moments becomes stronger due to the increasing overlap between Te $5p$ (Se $4p$) and Fe $3d$ orbitals. However, the effective charge transfer from Te to Fe shifts the density of states (DOS) to lower energies, depleting DOS at E_F thus weakening the longer-range magnetic interaction mediated by itinerant electrons. As a result, as $h_{Se/Te}$ is lowered below a critical value, the magnetic ground state switches from double-stripe $(\pi, 0)$ to single-tripe (π, π) magnetic ordering, allowing a greater probability of (π, π) spin fluctuation for realizing superconductivity. However, although the origin of superconductivity is believed to be magnetic in general and (π, π) spin fluctuation in particular, we note that $h_{Se/Te}$ could also affect DOS at E_F [31], carrier density, and nanoscale electronic inhomogeneity (e.g., the proximity effect between coexisting superconducting and semiconducting phases), which may also affect T_C. Doping experiments on $FeSe_{1-x}Te_x$ [10] and high-pressure measurements on FeSe [20] also indicate that reducing $h_{Se/Te}$ enhances T_C.

In high-pressure experiments on FeSe, all structural parameters decrease with increasing pressure. In contrast, a smaller $h_{Se/Te}$ accompanies a larger c axis and a larger $d_{Se\text{-}Se}$ in thin films. The structure becomes increasingly two dimensional and degrades superconductivity [20]. This is again consistent with our result that T_C exhibits a global maximum versus $\Delta h_{Se/Te}$ decreasing as the structure becomes more two dimensional.

In summary, we show that the substrate temperature can be exploited to apply well-defined stress to epitaxial $FeSe_{0.5}Te_{0.5}$ thin films on (100)MgO, where the lattice parameters, and more importantly, the Fe-Se(Te) tetrahedron are systematically varied within a single composition. Our results indicate that the superconducting transition temperatures of $FeSe_{0.5}Te_{0.5}$ thin films are linked to the chalcogen height.

The assistance of William Ratcliff at the NCNR is gratefully acknowledged. Work by S. X. H. and C. L. C. is supported by the NSF under DMR-0520491 and work by V. T. and C. B. is supported by the DOE under DE-FG02-08ER46544.

[1] Y. Kamihara *et al.*, J. Am. Chem. Soc. **130**, 3296 (2008).
[2] X. H. Chen *et al.*, Nature (London) **453**, 761 (2008).
[3] F.-C. Hsu *et al.*, Proc. Natl. Acad. Sci. U.S.A. **105**, 14 262 (2008).
[4] T. Y. Chen *et al.*, Nature (London) **453**, 1224 (2008).
[5] I. I. Mazin *et al.*, Phys. Rev. Lett. **101**, 057003 (2008).
[6] V. Cvetkovic and Z. Tesanovic, Europhys. Lett. **85**, 37 002 (2009).
[7] F. Wang *et al.*, Phys. Rev. Lett. **102**, 047005 (2009).
[8] A. V. Chubukov, D. V. Efremov, and I. Eremin, Phys. Rev. B **78**, 134512 (2008).
[9] C.-Y. Moon and H. J. Choi, Phys. Rev. Lett. **104**, 057003 (2010).
[10] K. Horigane, H. Hiraka, and K. Ohoyama, J. Phys. Soc. Jpn. **78**, 074718 (2009).
[11] K. Kuroki *et al.*, Phys. Rev. B **79**, 224511 (2009).
[12] E. Bellingeri *et al.*, Supercond. Sci. Technol. **22**, 105007 (2009).
[13] Y. Han *et al.*, J. Phys. Condens. Matter **21**, 235702 (2009).
[14] W. Si *et al.*, Appl. Phys. Lett. **95**, 052504 (2009).
[15] M. J. Wang *et al.*, Phys. Rev. Lett. **103**, 117002 (2009).
[16] Y. Imai *et al.*, arXiv:0910.2301.
[17] T. M. McQueen *et al.*, Phys. Rev. B **79**, 014522 (2009).
[18] C. Friesen and C. V. Thompson, Phys. Rev. Lett. **89**, 126103 (2002).
[19] K. Kusaka *et al.*, J. Vac. Sci. Technol. A **22**, 1587 (2004).
[20] S. Margadonna *et al.*, Phys. Rev. B **80**, 064506 (2009).
[21] S. Medvedev *et al.*, Nature Mater. **8**, 630 (2009).
[22] K.-W. Yeh *et al.*, Europhys. Lett. **84**, 37 002 (2008).
[23] Y. Mizuguchi *et al.*, J. Phys. Soc. Jpn. **78**, 074712 (2009).
[24] B. C. Sales *et al.*, Phys. Rev. B **79**, 094521 (2009).
[25] S. X. Huang and C. L. Chien (unpublished).
[26] M. Birkholz, *Thin Film Analysis by X-Ray Scattering* (Wiley-VCH, Weinheim, 2006), p. 36.
[27] B. Lebech and M. Nielsen, RCN-234, Proc Neutron Diffraction Conf. (Petten), p. 466 (1975).
[28] S. Li *et al.*, Phys. Rev. B **79**, 054503 (2009).
[29] K. Nakayama *et al.*, arXiv:0907.0763.
[30] H. A. Mook *et al.*, arXiv:0904.2178.
[31] E. Z. Kuchinskii *et al.*, arXiv:1004.0801.